ELSEVIER

International Journal of Heat and Fluid Flow 19 (1998) 492–504

International Journal of HEAT AND FLUID FLOW

Spectral-dynamic model for LES of free and wall shear flows

J.H. Silvestrini [a,b], E. Lamballais [a,c], M. Lesieur [a,*]

[a] LEGI/IMG (URA-CNRS) INPG–UJF, BP53, 38041 Grenoble Cedex 09, France
[b] DMPA/CPGMAp/UFRGS, Av. Bento Goncalves 9500, 91501-970 Porto Alegre, RS, Brazil
[c] LEA/CEAT, 43, Route de l'Aérodrome, 86036 Poitiers Cedex, France

Abstract

Using EDQNM nonlocal spectral expansions, we have developed a spectral-dynamic model for LES of turbulence, allowing to account for kinetic-energy spectra steeper than Kolmogorov at the cutoff. In the case of a temporal mixing layer forced by a weak 3D isotropic white noise, a self-similar state is reached, statistically in good agreement with laboratory experiments, except for kinetic-energy spectra which behave like k^{-2} at the cutoff, instead of $k^{-5/3}$. The pressure spectrum is compared with quasi-normal predictions. Concerning coherent-vortex dynamics, the helical-pairing organization already found with the aid of DNS has been recovered. When the initial forcing is quasi 2D, no self-similar state is reached. Coherent vortices consist then of quasi two-dimensional Kelvin–Helmholtz billows with hairpin vortices stretched in-between. Afterwards, the model has been applied successfully to a turbulent channel flow at $h^+ = 204$ and $h^+ = 389$. In the latter case, the computing time is reduced by a factor of 100 with respect to DNS. The model works also well for LES of a channel rotating about a spanwise axis. Finally, we have proposed a generalization of the spectral-dynamic model in physical space. © 1998 Elsevier Science Inc. All rights reserved.

Keywords: Subgrid-scale models; Large-eddy simulations; Vortex dynamics; Temporal mixing layer; Turbulent channel; Spanwise rotation

1. Introduction

Generally, the subgrid-scale modelling problem in Large-Eddy Simulations (LES) of turbulence is posed in physical space. This has two major drawbacks: first, it obliges to use an eddy-viscosity assumption, which is widely recognized as being unsatisfactory, since it assumes in fact a separation of scales between resolved and subgrid scales. Second, simulations in physical space prevent the use of pseudo-spectral methods, which are however much more precise than finite-difference or finite-volume methods. This is why in the present paper we will mainly work in Fourier space, and use a particular type of spectral eddy viscosity able to deal both with transitional situations and the proximity of a wall. We will present the spectral-dynamic model, and apply it to a temporal mixing layer (forced by a 3D or a quasi 2D random perturbation) and a channel flow (non-rotating or rotating). We will be interested by statistical predictions and by coherent-vortex dynamics as well. We will also look briefly how the spectral-dynamic model may be implemented in physical space.

2. The spectral-dynamic model

We start by considering the LES problem from a spectral point of view, with a sharp cutoff above k_c in Fourier space in a context of homogeneous and isotropic turbulence (Lesieur, 1997). Following the concept of spectral eddy viscosity introduced by Kraichnan (1976), Chollet and Lesieur (1981) have proposed to renormalize the eddy viscosity with the aid of $[E(k_c,t)/k_c]^{1/2}$, where $E(k,t)$ is the kinetic-energy spectrum. More precisely, the eddy viscosity in spectral space writes

$$\nu_t(k,k_c,t) = K(k/k_c)\ \nu_t^{\infty}(k_c,t) \tag{1}$$

with

$$\nu_t^{\infty}(k_c,t) = 0.267\left[\frac{E(k_c,t)}{k_c}\right]^{1/2}, \tag{2}$$

$$K(k/k_c) = 1 + 34.5\ \mathrm{e}^{-3.03(k_c/k)}. \tag{3}$$

The constant 0.267 was obtained with the aid the Eddy-Damped Quasi-Normal Markovian (EDQNM) nonlocal-interactions theory (see Chollet and Lesieur, 1981; Lesieur, 1997), using leading-order expansions in powers of the small parameter k/k_c, and assuming that $E(k)$ follows a Kolmogorov law extending above the cutoff. In Eq. (3), $K(k/k_c)$ displays a strong overshoot (cusp-behaviour) in the vicinity of $k/k_c = 1$, as shown by Kraichnan (1976). This is due to local or semi-local interactions in the neighbourhood of k_c. If one goes back to physical space, the plateau part of the spectral eddy viscosity corresponds to a classical eddy-viscosity formulation, which, as already stressed, assumes in fact a separation of scales between supergrid and subgrid scales. This is of course wrong, and fixes the limits of the eddy-viscosity formulation. Therefore, the cusp part of the spectral eddy viscosity is im-

* Corresponding author. E-mail: marcel.lesieur@hmg.inpg.fr.

0142-727X/98/$ – see front matter © 1998 Elsevier Science Inc. All rights reserved.
PII: S0142-727X(98)10029-2

portant since it contains effects beyond the classical eddy-viscosity concept.

The eddy-diffusivity was found to behave qualitatively the same (Chollet and Lesieur, 1982), with a corresponding turbulent Prandtl number $\mathrm{Pr}^t = \nu_t^\infty / k_t^\infty$ approximately constant and taken equal to 0.6 (see Lesieur, 1997, for details).

The major drawback of the eddy viscosity described by Eq. (1) is that it assumes a Kolmogorov spectrum at the cutoff. This condition is obviously not satisfied in transitional regions, or close to a wall even at high Reynolds numbers. In fact, let us express the EDQNM asymptotic spectral eddy viscosities and diffusivities $\nu_t^\infty(k_c,t)$ and $\kappa_t^\infty(k_c,t)$, still using leading-order expansions in powers of the small parameter k/k_c. We have

$$\nu_t^\infty(k_c,t) = \frac{1}{15}\int_{k_c}^{\infty} \theta_{0pp}\left[5E(p,t) + p\frac{\partial E}{\partial p}\right] \mathrm{d}p \tag{4}$$

and

$$\kappa_t^\infty(k_c,t) = \frac{2}{3}\int_{k_c}^{\infty} \theta_{0pp}^{\mathrm{T}}\, E(p,t)\, \mathrm{d}p, \tag{5}$$

where θ_{kpq} and $\theta_{kpq}^{\mathrm{T}}$ are nonlinear triple-correlation relaxation times of the EDQNM theory. The eddy coefficients may now be evaluated in a less restrictive context than previously. Assuming that the kinetic energy spectrum follows a power law $E(k) \propto k^{-m}$ instead of a Kolmogorov law, we find (for $0 < m < 3$):

$$\nu_t^\infty(k_c,t) = 0.31\; C_k^{-3/2}\; \frac{5-m}{m+1}\; (3-m)^{1/2}\; \left[\frac{E(k_c,t)}{k_c}\right]^{1/2} \tag{6}$$

with the associated turbulent Prandtl number

$$\mathrm{Pr}^t = 0.18\; (5-m). \tag{7}$$

The above scaling is not valid for $m > 3$. The eddy viscosity and diffusivity (normalized by $[E(k_c,t)/k_c]^{1/2}$) as a function of m are presented on Fig. 1. One can observe on this graph that ν_t^∞ and k_t^∞ decrease monotonously in the interval $0 < m < 3$. It is interesting to note that ν_t^∞ is reduced by more than 50% with respect to its value for $m = \frac{5}{3}$, as soon as $m > 2.2$, and multiplied at least by a factor of 2 if $m < 1$.

In the "spectral dynamic model" used for the LES presented below, the spectral eddy viscosity is defined with the aid of Eqs. (1) and (6). Thus, the k-dependence of the eddy-viscosity have been conserved through (3). As already stressed, it is important to keep the cusp, in order to avoid the classical eddy-viscosity assumption. Using the spectral-dynamic model permits also to reduce automatically the eddy viscosity without any empirical correction (like adjustment of constant(s) in the model) in the following two situations.

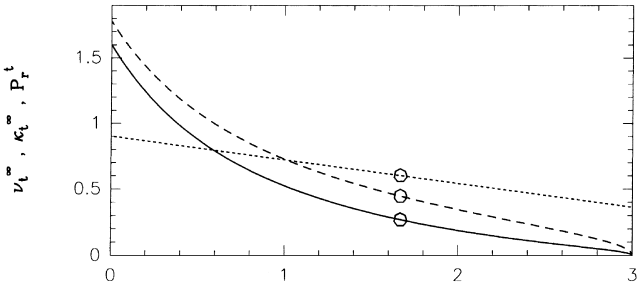

Fig. 1. Variation with m (the slope of the kinetic-energy spectrum at the cutoff) of the eddy viscosity and diffusivity (normalized by $[E(k_c,t)/k_c]^{1/2}$) and turbulent Prandtl number. Symbols correspond to $m = \frac{5}{3}$. ———: ν_t^∞, - - - -: k_t^∞,.....: Pr^t.

- For transitional or moderate Reynolds number flows, where no inertial zone can exist in the kinetic energy spectrum.
- For near-wall region of fully turbulent flows, where kinetic energy spectra are steeper than Kolmogorov, even at high Reynolds number.

Note that Eq. (6) is only valid for $m \leqslant 3$. For $m > 3$, our choice was to set the eddy-viscosity equal to zero. From a practical viewpoint, this may be justified by considering that if the kinetic energy spectrum is steep enough, there is no energy pile-up at high wave numbers, so that no subgrid-scale modelling is really necessary. Note finally that for numerical codes based on spectral methods as in the following sections, the spectral-dynamic model is very easy to use, with a negligible extra computational cost (less than 1% of the total computational cost of a LES).

3. Application to mixing layer

3.1. Flow configuration and numerical aspects

Two LES of temporal mixing layers differing only in the initial perturbations from a hyperbolic-tangent velocity profile $U \tanh y/\delta_0$ were carried out. The initial Reynolds numbers in the two cases are $\mathrm{Re}_{\delta_i} = U\delta_i/\nu = 2000$, where $\delta_i = 2\delta_0$ is the initial vorticity thickness. We denote by $\omega_i = 2U/\delta_i$ the initial maximal vorticity modulus (vorticity at the inflexion point).

The filtered Navier–Stokes equations are solved in a cubic computational domain of side $L_x = L_y = L_z = 4\ \lambda_a$, where $\lambda_a = 7\ \delta_i = 2\pi/k_a$ is the wavelength of the most amplified streamwise mode predicted by the inviscid linear-stability theory (Michalke's mode). Such a domain allows thus for two successive pairings of Kelvin–Helmholtz (KH) vortices during a simulation. Periodic boundary conditions are imposed in the streamwise (x) and spanwise (z) directions, while free-slip boundary conditions are employed for $y = \pm L_y/2$. Pseudo-spectral methods are used to solve the equations for the explicit velocity $\hat{\mathbf{u}}(\mathbf{k},t)$ in Fourier space:

$$\left[\frac{\partial}{\partial t} + (\nu + \nu_t(k,k_c,t))\; k^2\right]\hat{\mathbf{u}}(\mathbf{k},t) = \Pi\left[F\left[F^{-1}\left(\hat{\mathbf{u}}(\mathbf{k},t)\right) \times F^{-1}\left(i\mathbf{k}\times\hat{\mathbf{u}}(\mathbf{k},t)\right)\right]\right], \mathbf{k}\cdot\hat{\mathbf{u}}(\mathbf{k},t) = 0, \tag{8}$$

where F stands for the discrete Fourier transform operator and Π is the projector on the plane normal to the wavevector $\mathbf{k}$, allowing to eliminate the pressure. Note that free-slip boundary conditions are verified by means of pure sine or cosine expansions in the y-direction. The equations are integrated in time using a third-order low-storage Runge–Kutta scheme (Williamson, 1980). Aliasing errors (Canuto et al., 1988) are minimized by taking more collocation points in physical space (120^3) than Fourier modes (96^3).

Initial conditions consist in superposing to a basic hyperbolic-tangent velocity profile two types of random perturbations

- a small three-dimensional Gaussian isotropic perturbation of kinetic energy $10^{-4}U^2$, for the first simulation referred to as the "3D Perturbation Case";
- a combination of two perturbations: one two-dimensional (without any dependence on the spanwise direction) of kinetic energy $10^{-4}U^2$ plus a three-dimensional of kinetic energy $10^{-5}U^2$, for the second simulation called "Q2D Perturbation Case".

The simulations were stopped at $t = 60\ \delta_i/U$ (for the 3D Case) and 85 δ_i/U (for the Q2D Case). No confinement effects on the mixing layers were observed. At these times, the Rey-

nolds number based on the local vorticity thickness δ (defined as $2U/|\langle\omega_z\rangle(y=0)|$) was $\mathrm{Re}_\delta = 24\,000$ for the two simulations.

In these LES, the spectral-dynamic model is used in its "standard" version defined by Eqs. (1), (3) and (6). The spectrum slope m is calculated at each time step (and at each sub-step of the Runge–Kutta method), from the three-dimensional kinetic energy spectrum in the whole domain, using a least-square method applied to wave numbers ranging between $k_c/2 < k < k_c$.

3.2. 3D perturbation case

3.2.1. Model validation and statistical results

Fig. 2 shows the temporal evolution of m and $E(k_c)$ for the whole simulation. The spectrum slope decreases initially from the high initial value ($m \approx 9$). At $t = 10\ \delta_i/U$, which correspond to the time of the vortex roll-up, we have $m \approx 3$. It means that the eddy-viscosity was inactive (see Eq. (6)) up to this instant, and that all the dissipation was due to molecular viscosity. Hence instabilities are allowed to grow without any influence of the eddy viscosity, which is certainly desirable. Between $t = 10$ and $30\ \delta_i/U$ (moment of the first pairing), the slope m decreases from 3 to 2. After that, m remains very close to 2 up to the end of the simulation. The temporal evolution of $E(k_c)$, which reaches its maximum at $t = 25\ \delta_i/U$ and then decreases slowly, might indicates that a "quasi-equilibrium state" characteristic of the self-similar regime was attained.

Statistics of the recorded velocity profiles were used to determine the temporal evolution of the local vorticity thickness, and compared with experimental data of spatially-growing mixing layers carried out by Bell and Mehta (1990). The l.h.s. of Fig. 3 shows $\delta(t)$. A fairly good linear growth is established very early at a rate of $U^{-1}\mathrm{d}\delta/\mathrm{d}t = 0.19$. For an associated spatial mixing layer between two streams of velocities v_1 and v_2 with $v_1 - v_2 = 2u$, and with the change of variable $x = \frac{1}{2}(u_1 + u_2)t$, this corresponds to the growth rate $[(u_1 - u_2)/(u_1 + u_2)]\,\mathrm{d}\delta/\mathrm{d}x = 0.19$. During the first pairing ($t \approx 30$), the spreading slows down, and then it starts rising again at the same linear rate. In spite of the differences in the growth of spatial mixing layers reported in several works (Silvestrini, 1996), and also between the spatial and the temporal problems, the value found here is very close to the traditionally accepted result of 0.18 reported in Brown and Roshko's experiments (Brown and Roshko, 1974). The r.h.s. of Figs. 3 and 4 show, respectively, the mean streamwise velocity and velocity-component variances at the end of the simulation ($t = 60\ \delta_i/U$). The agreement between numerical and experimental data is good. The small differences, especially for $\langle u'u'\rangle$ and $\langle u'v'\rangle$, may be due to a lack of convergence because only spatial averages in periodic directions are used for

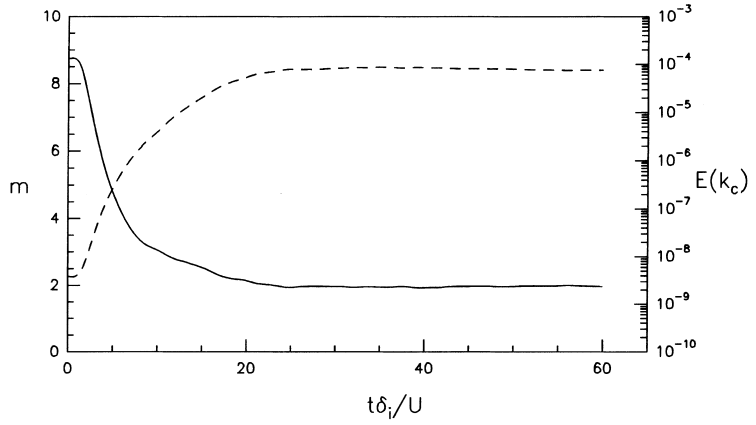

Fig. 2. 3D mixing layer; time evolution of m (——) and $E(k_c)$ (- - -).

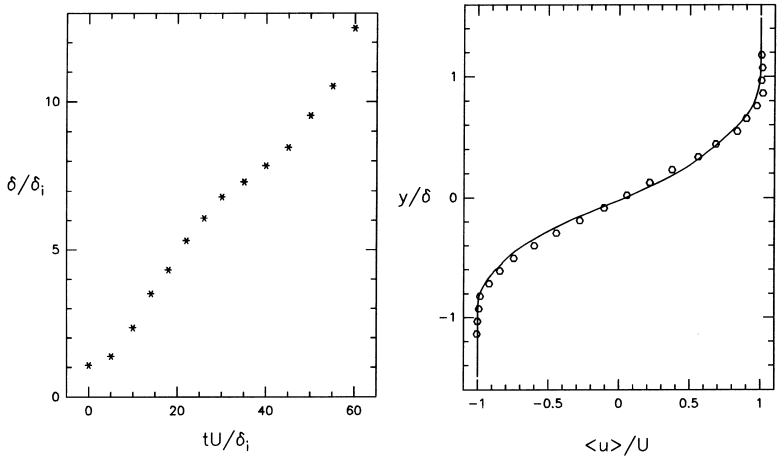

Fig. 3. 3D mixing layer; left, time evolution of the local vorticity thickness; right, comparison of mean streamwise velocity (straight line) with experimental data of Bell and Mehta (1990) (circles).

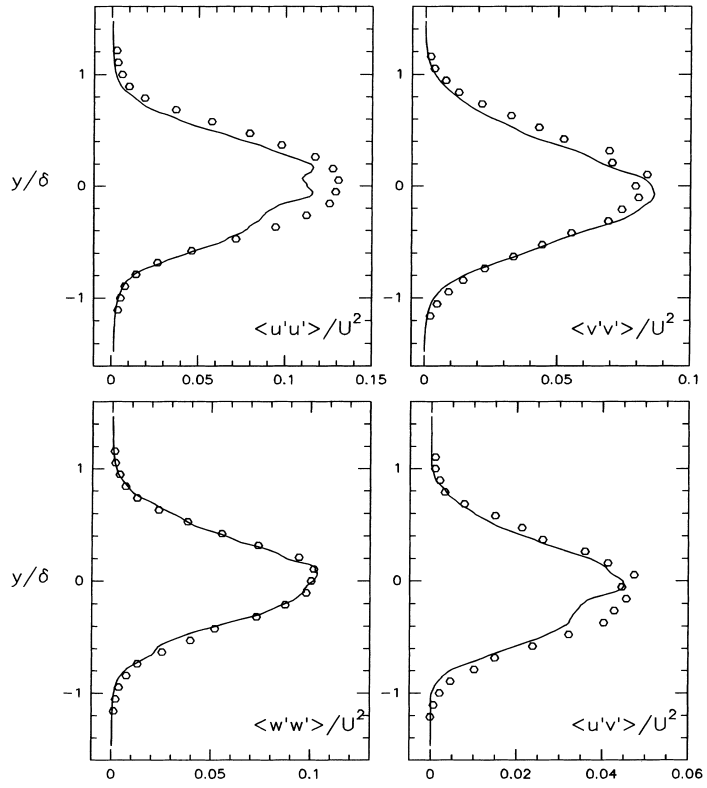

Fig. 4. 3D mixing layer; comparison of present velocity fluctuations variances (lines) with experimental data (symbols) of Bell and Mehta (1990).

present results. This good agreement seems to indicate that a self-similar state has been established at the end of the simulation. To confirm this point, normalized three-dimensional kinetic energy spectra are presented in Fig. 5 (the normalization is made by U and the local vorticity thickness δ). The good collapse of the different spectra for $t = 50$, 55 and 60 δ_i/U is another good indicator of self-similarity. Note also that Bell and Metha have considered that a self-similar regime was established at a streamwise distance of about 250 δ_i from the splitter plate, with a velocity ratio $\lambda = (U_1 - U_2)/(U_1 + U_2) = 0.25$. With the above introduced space-time change of variables, and using the convection velocity $U_c = (U_1 + U_2)/2$, we have

$$t_{\text{self}} = \frac{x_{\text{self}}}{U_c} = \lambda \, \frac{x_{\text{self}}}{U}, \tag{9}$$

and the value found $t_{\text{self}} = 62.5 \; \delta_i/U$ is very close to the time considered for present statistics.

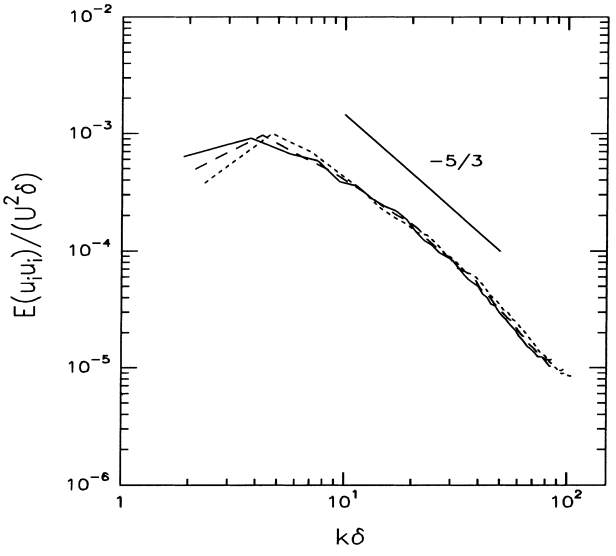

Fig. 5. 3D mixing layer, normalized three-dimensional kinetic energy spectra at $t = 50$ (——), 55 (- - -) and 60 δ_i/U (- - -).

The principal disagreement with experiments concerns the spectral slope of the kinetic-energy spectrum. Indeed, mixing-layer experiments at this Reynolds number do possess a very good $k^{-5/3}$ Kolmogorov law over a quite long range at large wave numbers. In our results, a Kolmogorov law may be observed (see Fig. 5) only over a short range, whereas the slope is steeper near k_c (close to 2, in agreement with Fig. 2). We had already observed this defect in LES of isotropic turbulence using the plain spectral-cusp model (with a fixed parameter $m = \frac{5}{3}$), and also the present spectral-dynamic model (Ossia, 1997). Therefore, it is clear that the extra reduction of the eddy-viscosity brought by the slope −2 is not sufficient to permit the establishment of an exact Kolmogorov cascade at k_c.

Since the spectral-dynamic model enables us to find good estimates of second-order velocity moments, it is interesting to examine higher order velocity moments as well as pressure statistics. The 3rd and 4th order moments of the streamwise velocity fluctuations at the end of the simulation are presented in Fig. 6. No self-similar state was attained at these moments, and longer simulations are necessary. Note however that present statistics allow to observe the non-Gaussian character in the intermittency zone between rotational and irrotational fluid out of the mixing layer. On the other hand, we have $\langle u'^3 \rangle \approx 0$ and $\langle u'^4 \rangle / \langle u'^2 \rangle^2 \sim 3$ in the middle of the shear layer, indicating a Gaussian behaviour. The curves are qualitatively similar to the ones determined experimentally by Spencer and

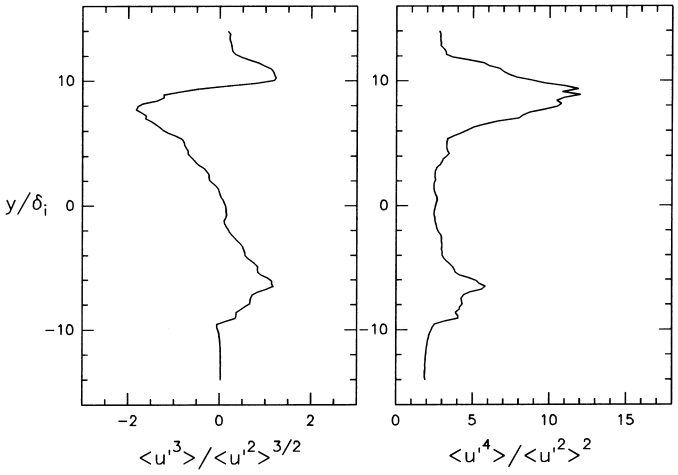

Fig. 6. 3D mixing layer; third- (left) and fourth-order (right) moments for the streamwise velocity fluctuation at $t = 60\ \delta_i/U$.

Jones (1971), but the maximum values, localized at the edges of the mixing layer, are higher than the experimental ones.

Another interesting feature is the behaviour of the mean and fluctuating pressure. Fig. 7 shows their vertical distribution at the end of the simulation. Since the pressure gradient in a vortex tube is directed towards the exterior of the tube, the mean pressure profile is minimum at the middle of the mixing layer, where the vorticity imposed by the KH vortices is maximum. As seen previously for high-order velocity moments, no self-similar state can be observed for the fluctuating pressure variance, indicating that the second-order moment of pressure fluctuations takes more time to become self-similar than its velocity counterpart. We find at the end of the simulation $\langle p' \rangle / (\rho U^2) = 0.14$, which is close to the value 0.11 determined experimentally by Spencer and Jones (1971). Fig. 8 shows the pressure spectrum $E_{pp}(k)$ at $t = 60\ \delta_i/U$. We recall the $k^{-7/3}$ Batchelor–Oboukhov's law (see, e.g., Batchelor, 1953) for isotropic homogeneous turbulence, where one assumes a Kolmogorov law for the kinetic-energy spectrum and makes a quasi-normal evaluation of the fourth-order velocity correlations. In fact, this analysis leads to

$$E_{pp}(k) \sim k[E(k)]^2. \tag{10}$$

Such a law is still under debate for isotropic turbulence. For the mixing layer, it is clear from Fig. 8 that no $k^{-7/3}$ pressure spectrum exists, and that we are not far from a $k^{-5/3}$ law for the pressure. This shows that the quasi-normal assumption leading to Eq. (10) is not valid.

3.2.2. Coherent-vortex dynamics

Let us look now at the three-dimensional vortical structure. Fig. 9 presents a perspective view of vorticity-modulus isosurfaces (threshold $|\omega_i|$), at $t = 14$, 26, 40 and 60 δ_i/U. At $t = 14\ \delta_i/U$, one can see a dislocated array of four rolling-up Kelvin–Helmholtz vortices, similar to the configuration found in previous DNS of Comte et al. (1992) and laboratory experiments of Chandrsuda et al. (1978), and called "helical pairing". Secondaries streamwise vortices are also stretched by the deformation field induced between the big vortices. At $t = 26\ \delta_i/U$ large structures pair. The subsequent pairing is more difficult to identify from the vorticity isosurfaces, mainly because of a rapid growth of small-scale structures. At the end of the simulation ($t = 60\ \delta_i/U$), the vorticity field displays only the presence of intense small-scale vortices, with no obvious preponderant orientation. By contrast, the low-pressure field (see Fig. 10) indicates the presence of one big quasi two-dimensional vortex, stretching thinner longitudinal vortices. Note however that the computational domain is too small at this instant, with regard to the vortex size.

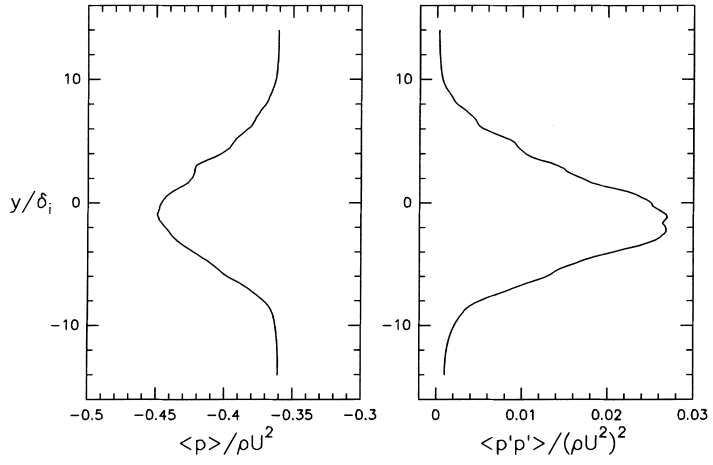

Fig. 7. 3D mixing layer; mean (left) and pressure variance (right) at $t = 60\ \delta_i/U$.

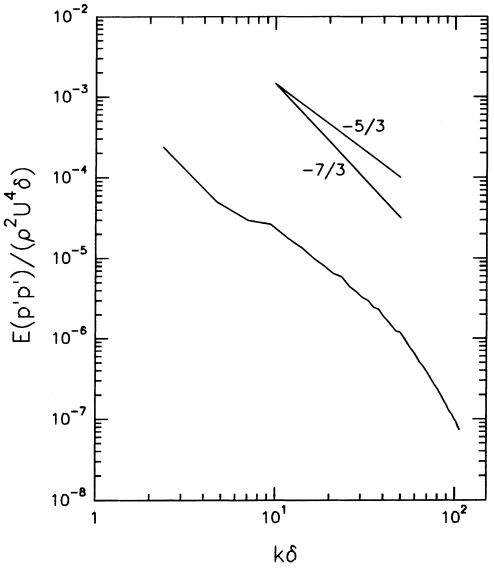

Fig. 8. 3D mixing layer; normalized three-dimensional pressure spectrum at $t = 60\ \delta_i/U$.

3.3. Q2D perturbation case

3.3.1. Model validation and statistical results

The time evolution of the slope m of the three-dimensional kinetic energy spectrum close to the cutoff and of $E(k_c)$ is presented in Fig. 11. Until $t = 10\ \delta_i/U$ the eddy viscosity is inactive since $m \leqslant 3$. Between $t = 10\ \delta_i/U$ (time of KH vortices roll-up) and $20\ \delta_i/U$ (beginning of the first pairing), the slope takes a rather constant value of $m = 2.5$. After that, and until the end of the simulation, m tends asymptotically to 2, the same value as in the previous 3D case. By contrast, the evolution of the kinetic-energy at k_c is different, since it keeps on increasing at the end of the simulation. This last observation suggests that no self-similar behaviour has been reached here.

The statistics of the second-order moments of the velocity confirm this idea. At the end of the simulation ($t = 85\ \delta_i/U$), their maximum values at the center of the mixing layer are: $\langle u'^2\rangle/U^2 = 0.20$, $\langle v'^2\rangle/U^2 = 0.20$, $\langle \omega'^2\rangle/U^2 = 0.17$ and $-\langle u'v'\rangle/U^2 = 0.08$. These values are higher than the self-similar ones obtained in the 3D Case and measured in Bell and Mehta's experiments (see Fig. 4).

3.3.2. Coherent-vortex dynamics

Fig. 12 shows vorticity-modulus isosurfaces of the quasi 2D mixing layer. The threshold value is $2|\omega_i|/3$ for $t = 14$ or

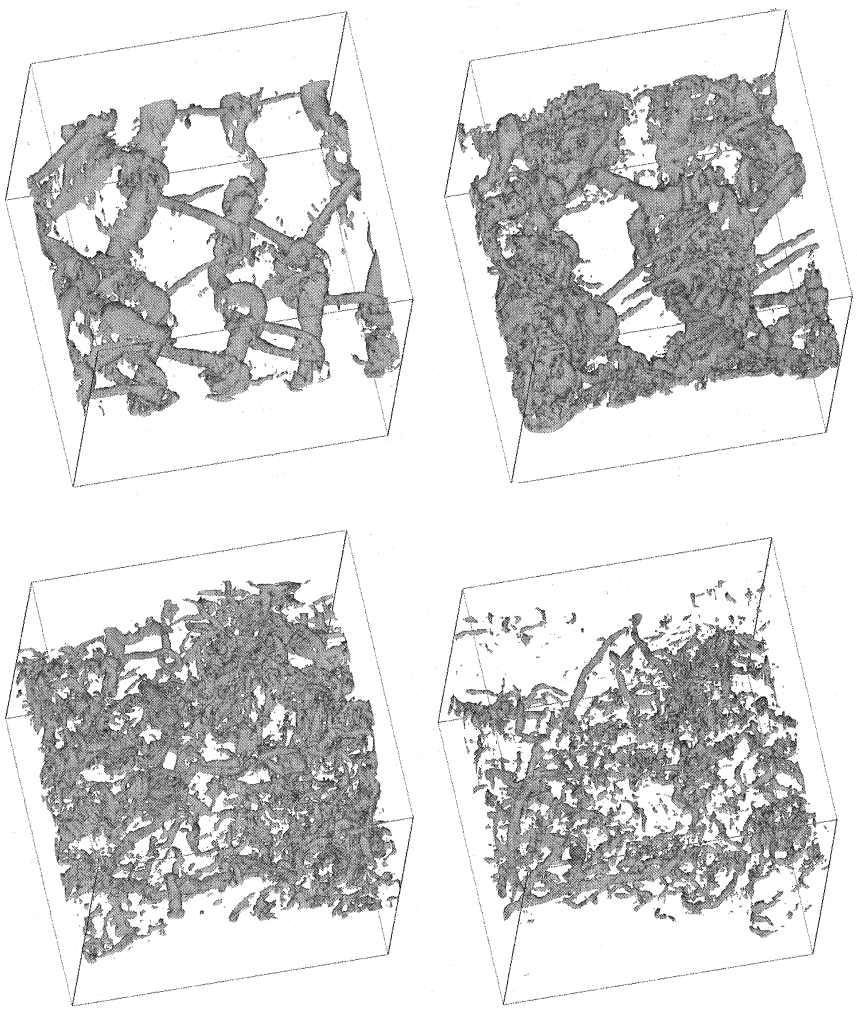

Fig. 9. 3D mixing layer; from left to right and top to bottom, perspective views at $t = 14$, 26, 40 and 60 δ_i/U showing isosurfaces of the vorticity modulus at a threshold of $|\omega_i|$.

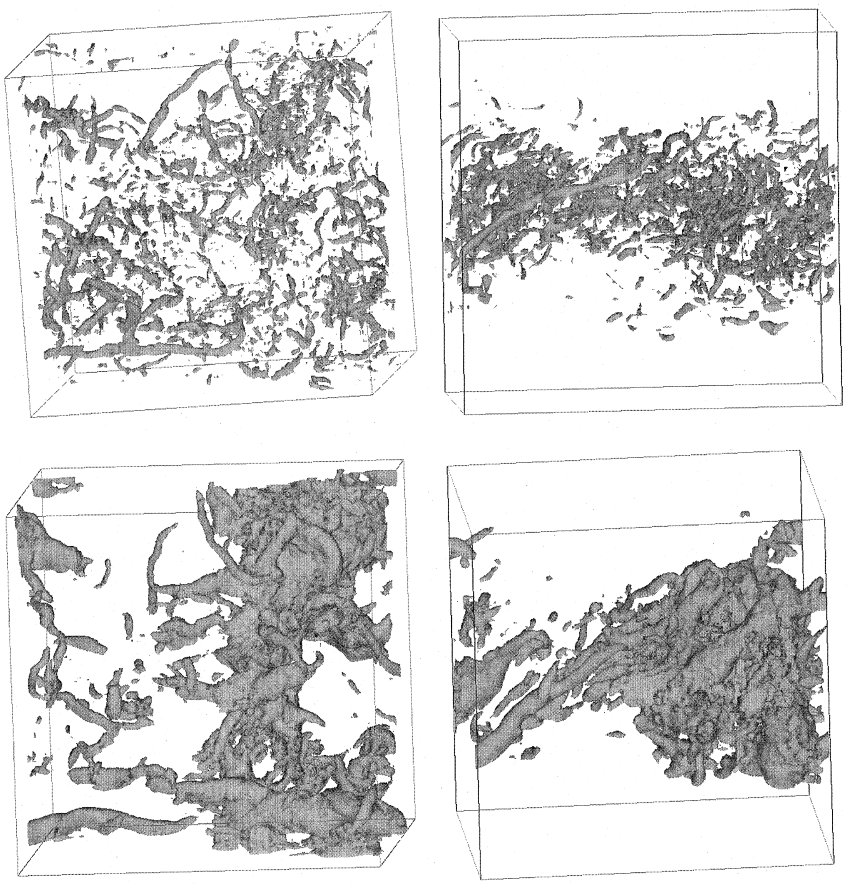

Fig. 10. Same as in Fig. 9 at $t = 60\ \delta_i/U$; top (left) and side (right) views of vorticity modulus (threshold 1.4 $|\omega_i|$, above) and low-pressure isosurfaces (bottom).

30 δ_i/U, and $|\omega_i|$ for $t = 45$ or 60 δ_i/U. The first pairing begins with the merging of the two central KH vortices at $t = 14\ \delta_i/U$ and finishes with the merging of the two exterior KH vortices at $t = 30\ \delta_i/U$. Intense streamwise vortices are stretched in the stagnation zone between the KH vortices, following a mechanism proposed by Lin and Corcos (1984). At $t = 45\ \delta_i/U$, the central KH vortex begins to oscillate in the spanwise direction, which seems to trigger the second pairing. At the end of the simulation, there is only one KH vortex, easily identified by isosurfaces of low pressure. Fig. 13 shows top and side views of the vorticity-modulus and low-pressure isosurfaces at $t = 85\ \delta_i/U$, when the simulation is stopped. The side views show the stretching of a hairpin vortex between the KH structures. This hairpin might result from the evolution of the large vortex oscillating in the spanwise direction observed before. Note finally the presence of intense small-scale vortices.

4. Application to channel flow

4.1. Flow configuration

In this section, the turbulent plane channel flow submitted (or not) to spanwise rotation is considered. Let $\langle \vec{u} \rangle = (\langle u \rangle, 0, 0)$

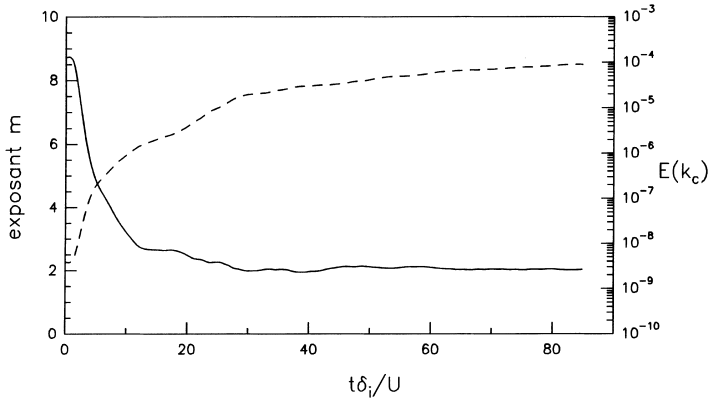

Fig. 11. Q2D mixing layer; time evolution of m (——) and $E(k_c)$ (- - -).

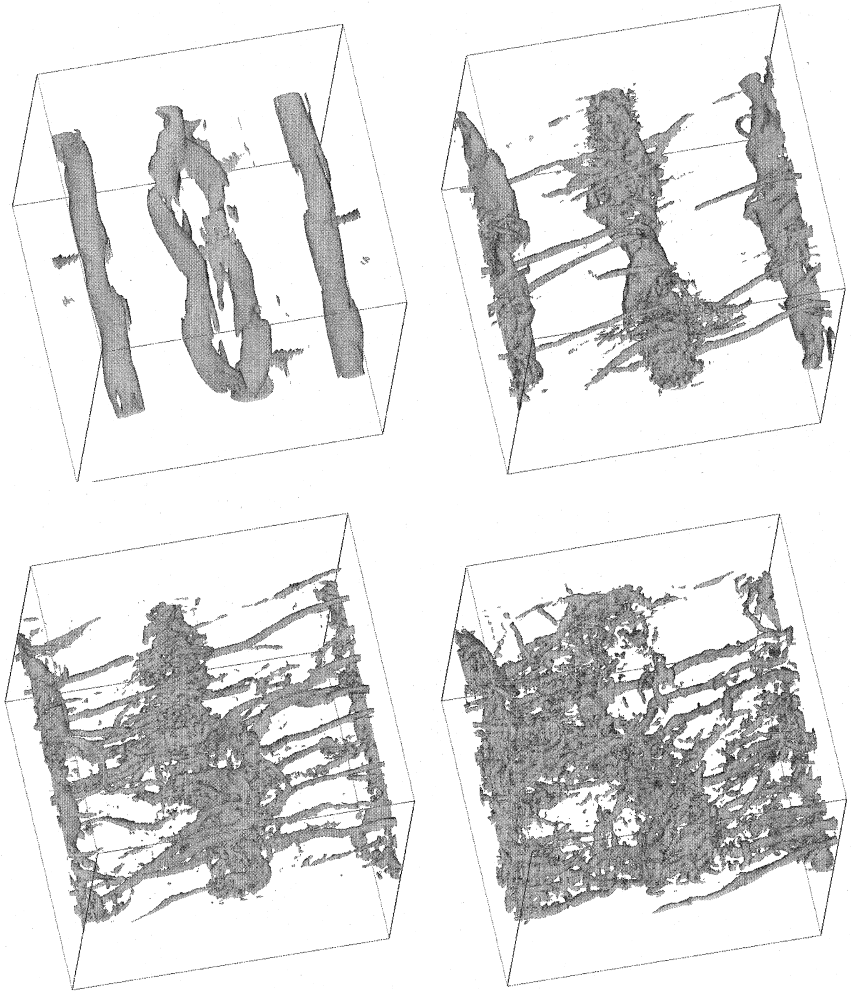

Fig. 12. Q2D mixing layer; from left to right and top to bottom, perspective views of the vorticity modulus for $t = 14$, 30 (threshold $2|\omega_i|/3$), 45 and 60 δ_i/U (threshold $|\omega_i|$).

be the mean relative velocity in a Cartesian coordinates system (x, y, z) associated to the rotating frame. x, y and z are respectively the streamwise, wall-normal and spanwise directions, the rotation vector being $\vec{\Omega} = (0, 0, \Omega)$ (see Fig. 14).

The half-channel height is noted h and the bulk velocity U_m. Non-dimensional parameters used here are the Reynolds number $\mathrm{Re} = U_m\, 2h/\nu$ and the global Rossby number $\mathrm{Ro_g} = 3\, U_m/(2\Omega\, h)$. Small values of the latter concern strong rotation regimes where Coriolis forces dominate inertial forces, while infinite global Rossby number corresponds to no rotation. Note that the $\frac{3}{2}$ factor in the global Rossby expression is consistent with a previous work where transitional rotating channel flow was considered (Lamballais et al., 1996b). In a laminar situation (Poiseuille flow), this global Rossby corresponds to the ratio of the vorticity at the wall ($3\, U_m/h$) upon the solid-body rotation vorticity 2Ω.

4.2. Model adaptation

An adaptation of the model formulation is necessary to treat the direction of inhomogeneity y. In the present case, two-dimensional spectra $E_{2\mathrm{d}}(y, k_{2\mathrm{d}}, t)$ have been used, with $k_{2\mathrm{d}} = \sqrt{k_x^2 + k_z^2}$. A slope $m(y, t)$ is then defined for each kinetic-energy spectrum in planes parallel to the walls, in such way that the spectral-eddy viscosity takes the final form

$$\nu_t^{\infty+}(y, k_{2\mathrm{d}}, t) = 0.31\; C_k^{-3/2}\; \frac{5 - m(y,t)}{m(y,t) + 1}\; [3 - m(y,t)]^{1/2} \times (1 + 34.5\mathrm{e}^{-3.03(k_\mathrm{c}/k_{2\mathrm{d}})})\; \left[\frac{E(y, k_\mathrm{c}, t)}{k_\mathrm{c}}\right]^{1/2}. \quad (11)$$

Note that the spectral formulation used in this model concerns only horizontal directions. Numerically, $m(y,t)$ is evaluated using a least-square method applied on a spectral range of highest wave numbers. For simulations presented here, a quite wide range of wave numbers has been considered ($k_\mathrm{c}/2 < k_{2\mathrm{d}} < k_\mathrm{c}$), but it has been verified that this range can be reduced without significant modification of the results.

A last remark concerns the use of a two-dimensional spectrum instead of a three-dimensional one. In an isotropic turbulence context, a 3D-spectrum $E(k) = c_1\, k^{-m}$ may be deduced from a 2D-spectrum $E_{2\mathrm{d}}(k_{2\mathrm{d}}) = c_2\, k_{2\mathrm{d}}^{-m}$ by integration: it is found

$$\frac{c_1}{c_2} = \left\{ \frac{\Gamma(\frac{1}{2})\Gamma(\frac{1}{2}(m+1))}{3\Gamma(\frac{1}{2}m+1)} - \frac{\Gamma(\frac{1}{2})\Gamma(\frac{1}{2}(m+1))}{6\Gamma(\frac{1}{2}m+2)} \right\}. \quad (12)$$

With the aid of this expression, it is possible to evaluate the 3D-spectrum at the cutoff wave number $E(k_\mathrm{c})$. Note however that this correction is not fully justified if the y-direction is inhomogeneous, as in the present situation. From a practical viewpoint, we have checked that use of the correction factor

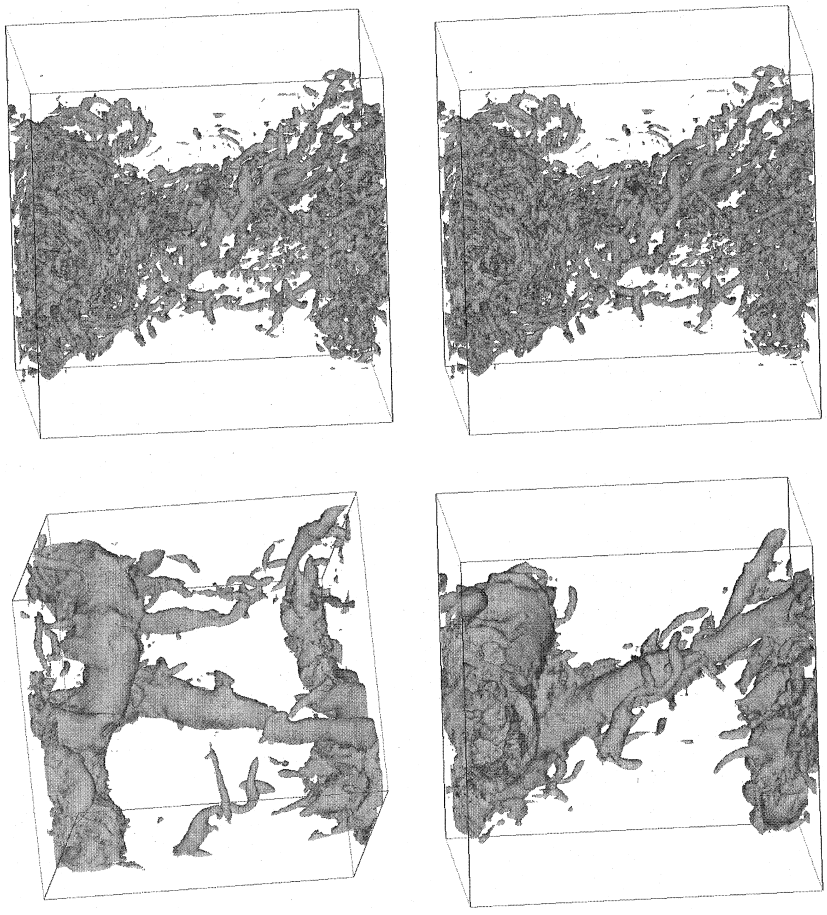

Fig. 13. Same as in Fig. 12 at $t = 85\ \delta_i/U$; top (left) and side (right) views of vorticity modulus (threshold $|\omega_i|$, above) and low-pressure isosurfaces (bottom).

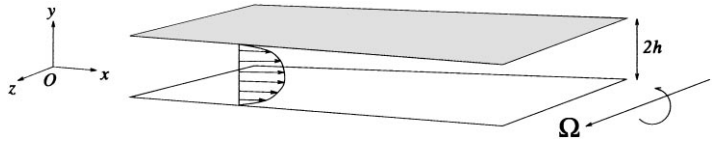

Fig. 14. Schematic view of the rotating channel.

given by Eq. (12) in the subgrid-scale model has a negligible effect on the final result.

4.3. Non-rotating channel

We use here a mixed spectral-compact code having quasi-spectral accuracy (see Lamballais, 1996, for details). We first present two LES of non-rotating channels at $\mathrm{Re} = 6666$ (case A) and $\mathrm{Re} = 14\ 000$ (case B). The grid refinement close to the wall allows to simulate accurately the viscous sublayer. The resolution is $(64 \times 65 \times 32)$ for case A, and $(128 \times 97 \times 64)$ for case B.

Fig. 15 shows the mean velocity profile in case A, compared with the LES of Piomelli (1993) using the dynamic model of Germano (1992). The latter is known to be in good agreement with experiments or DNS at this low Reynolds number. Present results coincide, with for instance correct values for the Karman constant or the friction velocity.

Fig. 16 shows for case A the rms velocity fluctuations, compared with Piomelli's results. The agreement is still very good, with a correct prediction of the longitudinal velocity fluctuations peak, corresponding to a maximum intensity of the high and low-speed streaks.

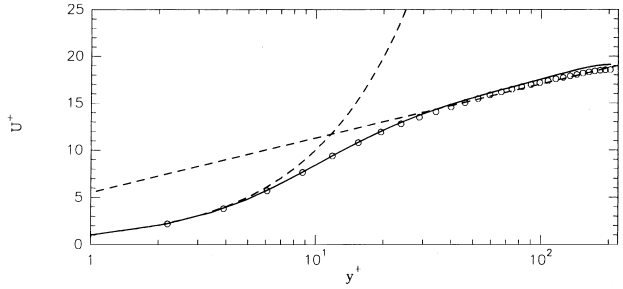

Fig. 15. Channel flow, $h^+ = 204$; comparison of the mean velocity profile (straight line) versus dynamic-model simulations of Piomelli (1993) (symbols).

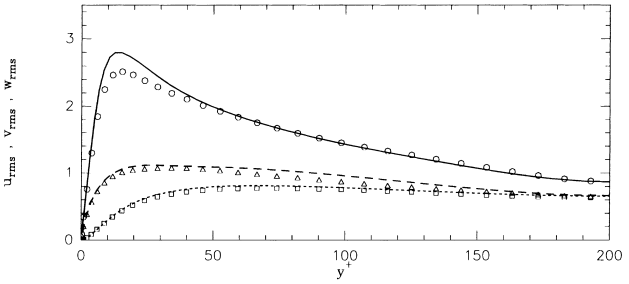

Fig. 16. Same as Fig. 15, but for the rms velocity fluctuations, from top to bottom longitudinal, spanwise and transverse velocities.

The same velocity statistics for case B are presented on Fig. 17 and compared with the DNS of Antonia et al. (1992) at approximately the same Reynolds number. It can be seen that mean velocity and turbulence intensities obtained by present LES are in good agreement with (unfiltered) DNS results. Notice that LES allow in this case to reduce the computational cost by a factor of nearly hundred with respect to the DNS.

Quality criteria based only upon statistics may be insufficient. Indeed, we have observed that a simulation without any subgrid-model (at the same Reynolds number and resolution) gives statistics of the velocity field (mean value, variances and Reynolds stresses) not dramatically affected, while kinetic-energy spectra or instantaneous vorticity fields are very unrealistic. Fig. 18 presents a vorticity visualization in the LES, compared with a DNS at lower Reynolds. The coherence of the large-scale motion in terms of hairpin ejections and streaks at the wall is preserved in the LES. It is clear also that LES indicate features expected from turbulence at higher Reynolds number, and display much more vortical activity in the small scales than the DNS. The small (resolved) scale activity thus predicted is susceptible of enhancing mixing or chemical reactions in LES of turbulent transport or combustion for instance.

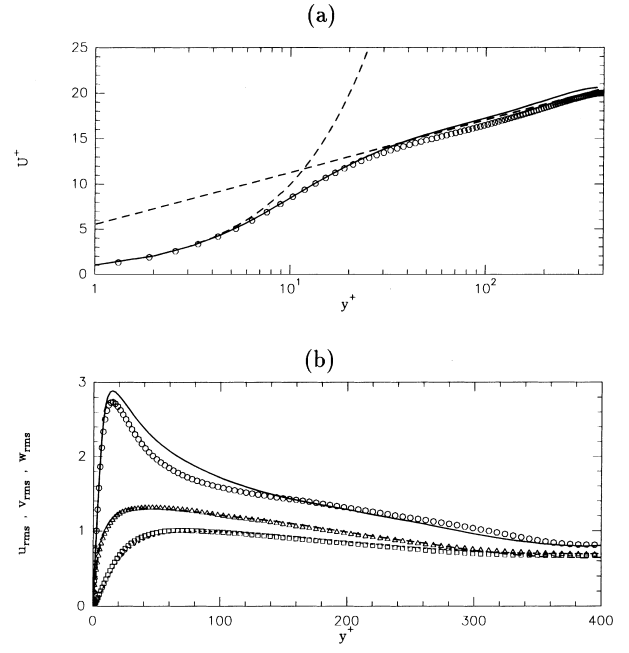

Fig. 17. Channel flow, comparisons of present LES using the spectral-dynamic model (straight lines, $h^+ = 389$) with the DNS of Antonia et al. (1992) (symbols, $h^+ = 395$); (a) mean velocity, (b) rms velocity components.

We have thus shown that the spectral-dynamic model gives a good near-wall behaviour in turbulent wall flows, without use of any "hand-tuned" constant in the eddy-viscosity formulation. To illustrate the importance of the eddy-viscosity correction, Fig. 19 shows the profile of the spectral exponent $m(y,t)$ averaged with time. It can be noticed first that spectra are clearly steeper than Kolmogorov in the whole channel. In addition, m is very close to 3 or higher in the viscous region, corresponding to a very low (or zero) value of the eddy viscosity. This permits correct near-wall statistics. Dynamic models in physical space present the same advantage, but not via an explicit control of the energy distribution in the highest wave numbers. Such a control may ensure a realistic decreasing kinetic energy spectrum near the cutoff wave number k_c, as we have noticed in all the large-eddy simulations performed with the spectral-dynamic model. In the present case, one should check on the experiments at this Reynolds number whether the quite steep velocity spectra obtained here are realistic, or if they are an artefact of the model. Indeed, we have seen above for the mixing layer or for isotropic turbulence that the spectral-dynamic model slightly overestimates the inertial-range exponents, from $\frac{5}{3}$ to 2.

4.4. Rotating channel results

The spectral-dynamic model has been also applied to the rotating turbulent channel (Lamballais, 1996; Lamballais et al., 1997), where results in good qualitative agreement with DNS at lower Reynolds numbers (Lamballais, 1996; Lamballais et al., 1996a) were obtained. The spectral-dynamic model is assessed here for a very strong rotation, corresponding to $\mathrm{Ro_g} = 2$. For such a rotation rate, DNS have shown that a quasi-laminar zone develops in the cyclonic region while, in the anticyclonic region, the vortex organization of the flow differs strongly from the non-rotating case. For present LES with higher Reynolds number, the same tendencies can be observed (see Fig. 20). For instance, a pdf analysis of the angle made by hairpins with the horizontal plane (not presented here) shows that vortices in the anticyclonic region lean more and more towards the wall as the Rossby number diminishes, while becoming more coherent.

To our knowledge, no equivalent DNS nor experiments at identical Reynolds number and rotation rate as present LES are given in the literature. Validation of the present simulation is therefore not yet feasible. It may be however interesting, at the same Rossby number, to compare DNS at lower Reynolds number ($\mathrm{Re} = 5000$) with present LES at $\mathrm{Re} = 14\,000$. Here, we concentrate our attention on the reduction of the cyclonic friction velocity (noted u_{τ_c}) with respect to its value without rotation (noted u_τ^∞) for the same Reynolds number. We find that this reduction is more marked for $\mathrm{Re} = 14\,000$ (LES) than for $\mathrm{Re} = 5000$ (DNS), with u_{τ_c}/u_τ^∞ respectively equal to 0.50 and 0.59. For moderate rotation ($18 < \mathrm{Ro_g} < 25$), Johnston et al. (1972) have reported the same tendency, i.e. a reduction of the normalized cyclonic wall friction with the increase of the Reynolds number ($\mathrm{Re} = 10\,300$ and $\mathrm{Re} = 11\,400$). Cyclonic friction velocity was found to be lower in these experiments than in DNS (Kristoffersen and Andersson, 1993; Lamballais, 1996). On the other hand, and for similar rotation rates, Launder and Tselepidakis (1994) in calculations using a one-point closure model, and Piomelli and Liu (1995) with LES, have noticed on the contrary an increase with the Reynolds number of the normalized friction velocity. Hence, further computations (very high resolution DNS) or experiments are necessary to decide about this point.

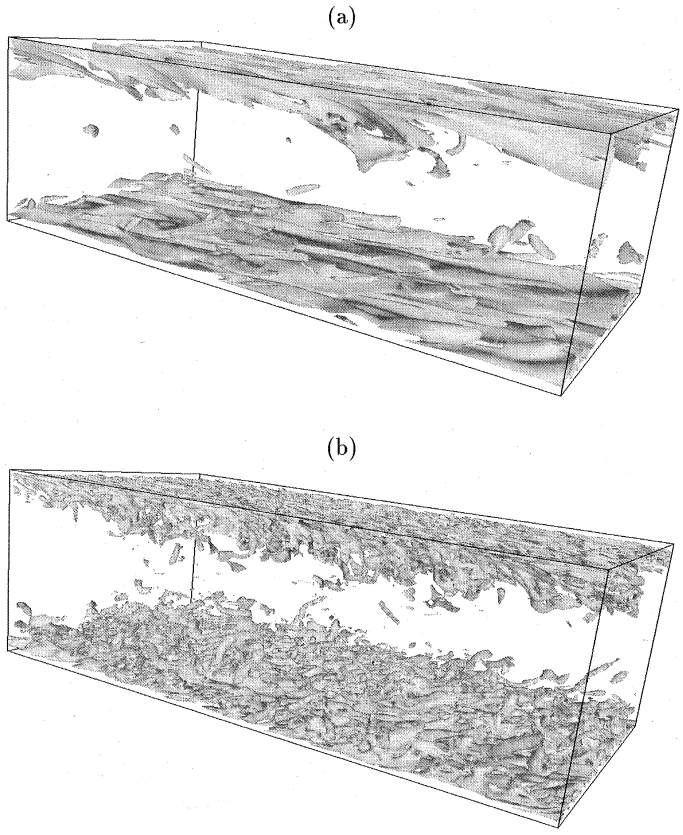

Fig. 18. Channel flow, isosurface of the vorticity modulus $\omega = 4.5\ U_m/h$; (a) DNS at $\mathrm{Re} = 5000$, (b) LES at $\mathrm{Re} = 14\,000$ (the flow goes from left to right).

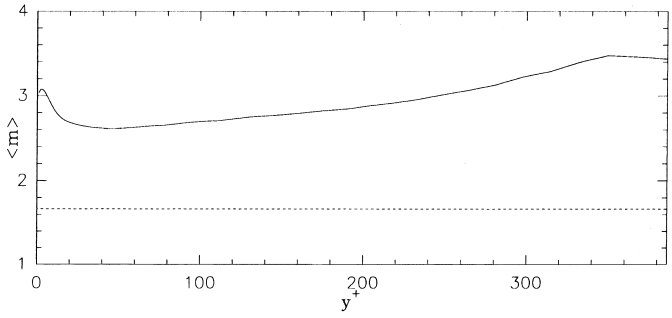

Fig. 19. Same LES as Fig. 17, profile of $\langle m \rangle$, the time-averaged value of the kinetic-energy spectrum slope, as a function of y^+.

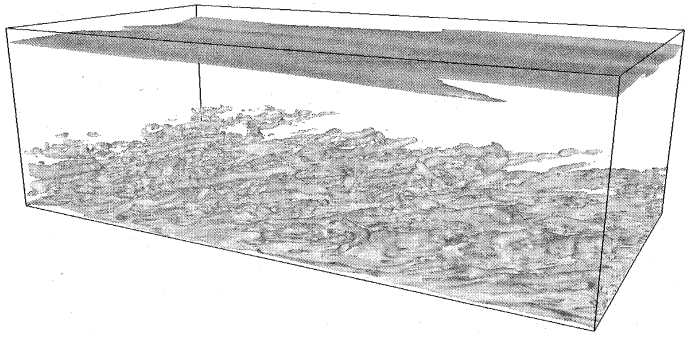

Fig. 20. LES of the rotating channel flow at $\mathrm{Re} = 14\,000$ and $\mathrm{Ro_g} = 2$; isosurface of the vorticity modulus $\omega = 3.375\ U_m/h$.

5. Return to physical space

In order to take into account the intermittency of turbulence, and to consider flows in complex geometries (without any periodic direction), a formulation of spectral dynamic model in physical space is naturally very useful. Three specific adaptations are then required, concerning

- the k-dependence of the eddy viscosity;
- the evaluation of the kinetic energy at the cutoff wave number k_c;
- the determination of the spectral slope m.

In fact, the k-dependence of the eddy viscosity defined by the function $K(x)$ in Eq. (3) can also be put under the form $K(x) = 1 + v_n^* x^{2n}$, with $2n \approx 3.7$ (Chollet and Lesieur, 1982). Determining v_n^* on the basis of subgrid-energy conservation (Métais, 1996), and approximating $2n$ by 4, one can propose an equivalent of the spectral-cusp model in physical space as

$$\frac{\partial \sigma_{ij}}{\partial x_j} = 0.661 \ \frac{\partial}{\partial x_j}\left[v_t^{SF}\left(\frac{\partial \bar{u}_i}{\partial x_j} + \frac{\partial \bar{u}_j}{\partial x_i} \right) \right] + 0.014 \ \Delta x^4 \ v_t^{SF} (\nabla^2)^3 \bar{u}_i, \tag{13}$$

where σ_{ij} is the traceless subgrid-scale tensor

$$\sigma_{ij} = T_{ij} - \frac{1}{3} T_{kk} \delta_{ij} \quad \text{with } T_{ij} = \overline{u_i}\ \overline{u_j} - \overline{u_i u_j}. \tag{14}$$

Here, v_t^{SF} is the eddy-viscosity of the structure-function model (Métais and Lesieur, 1992). This model has been applied with success by Garnier et al. (1998) for the study of the instability of a baroclinic jet resulting from a thermal front in a rotating stably-stratified atmosphere.

Multiplying the operator of Eq. (13) by $\tilde{A}$, with

$$\tilde{A} = \frac{2\sqrt{3}}{5} \ \frac{5-m}{m+1} \ (3-m)^{1/2}, \tag{15}$$

we obtain a subgrid-scale model defined in physical space and equivalent to the spectral-dynamic model. Strategies to evaluate m have to be developed.

6. Conclusions

With the aid of nonlocal spectral expansions of the EDQNM two-point closure theory of isotropic turbulence, we have developed a spectral-dynamic model for LES of turbulence. The model combines Kraichnan's plateau-cusp formulation with a correction accounting for kinetic-energy spectra which may behave differently from Kolmogorov at the cutoff. This model has been applied successively to a temporal mixing layer and a channel flow.

The mixing layer is forced initially by a hyperbolic-tangent velocity profile to which is superposed a weak random perturbation. Two cases have been considered: a 3D isotropic or a quasi 2D perturbation. In the 3D case, we converge towards a self-similar state in very good agreement with the laboratory experiments of Bell and Mehta (1990), as far as the growth rate, mean velocity, rms velocity and Reynolds-stress profiles are concerned. However, the kinetic-energy spectra behave like k^{-2} at the cutoff, instead of the $k^{-5/3}$ Kolmogorov law which is expected from the experiments at similar Reynolds numbers. Such a behaviour pertains in fact to the spectral-dynamic model, which gives similar results for isotropic turbulence. The pressure spectrum has a long range slightly shallower than $k^{-5/3}$, and in disagreement with predictions which can be made using quasi-normal assumptions. We have also looked at the dynamics of coherent vortices, with the aid of vorticity-modulus and low-pressure isosurfaces. We have recovered the helical-pairing organization, already found by Comte et al. (1992) using DNS with the same type of initial conditions. In the quasi 2D case, the simulation does not reach a self-similar state, and rms velocity statistics remain much higher than the experimental data. The kinetic-energy spectra are not very different from the 3D case. The coherent-vortex dynamics is made of quasi two-dimensional Kelvin–Helmholtz vortices stretching hairpin vortices between them.

For the plane Poiseuille flow, the spectral-dynamic model compares statistically very well with the Piomelli (1993) LES using the Germano (1992) dynamic model at $h^+ = 204$. It gives also good results at $h^+ = 389$, by comparison with the DNS of Antonia et al. (1992), although the computing time is reduced by a factor of the order of hundred. We have checked also that our model does not alter the coherent-structure dynamics, while allowing much more variability in the small scales at high Reynolds number. This last point may be important for LES of turbulent mixing or combustion. The case of a channel rotating rapidly about a spanwise axis has been considered, with results in good agreement with earlier experimental or numerical studies.

Finally, a generalization of the spectral-dynamic model in physical space in terms of a mixed structure-function and hyperviscosity has also been proposed.

Acknowledgements

We are grateful to P. Comte and O. Métais for useful discussions, and to P. Begou for computational assistance. Calculations were carried out at the IDRIS (Institut du Développement et des Ressources en Informatique Scientifique, Paris). This work was sponsored by Institut Universitaire de France, CNRS, INPG and UJF. The final version of this paper was prepared while the first author benefits from a FAPERGS (Brazil) research fellowship.

References

Antonia, R.A., Teitel, M., Kim, J., Browne, L.W.B., 1992. Low-Reynolds-number effects in a fully developed turbulent channel flow. J. Fluid Mech. 236, 579–605.

Batchelor, G.K., 1953. The Theory of Homogeneous Turbulence. Cambridge University Press, Cambridge.

Bell, J., Mehta, R., 1990. Development of a two-stream mixing layer from tripped and untripped boundary layers. AAIA J. 28, 2034–2042.

Brown, G., Roshko, A., 1974. On density effects and large structure in turbulent mixing layers. J. Fluid Mech. 64, 775–816.

Canuto, C., Hussaini, M.Y., Quarteroni, A., Zang, T.A., 1988. Spectral Methods in Fluid Dynamics. Springer, New York.

Chandrsuda, C., Mehta, R., Weir, A., Bradshaw, P., 1978. Effect of free-stream turbulence on large structure in turbulent mixing layers. J. Fluid Mech. 85, 693–704.

Chollet, J.P., Lesieur, M., 1981. Parameterization of small scales of the three-dimensional isotropic turbulence utilizing spectral closures. J. Atmos. Sci. 38, 2747–2757.

Chollet, J.P., Lesieur, M., 1982. Modélisation sous maille des flux de quantité de mouvement et de chaleur en turbulence tridimensionnelle isotrope. La Météorologie 29/30, 183–191.

Comte, P., Lesieur, M., Lamballais, E., 1992. Large- and small-scale stirring of vorticity and a passive scalar in a 3-d temporal mixing layer. Phys. Fluids A 4 (12), 2761–2778.

Garnier, E, Métais, O., Lesieur, M., 1998. Synoptic and frontal-cyclone scale instabilities in baroclinic jet flows. J. Atmos. Sci. 55, 1316–1335.

Germano, M., 1992. Turbulence: the filtering approach. J. Fluid Mech. 238, 325–336.

Johnston, J.P., Halleen, R.M., Lezius, R.K., 1972. Effects of spanwise rotation on the structure of two-dimensional fully developed turbulent channel flow. J. Fluid Mech. 56, 533–557.

Kraichnan, R.H., 1976. Eddy viscosity in two and three dimensions. J. Atmos. Sci. 33, 1521–1536.

Kristoffersen, R., Andersson, H.I., 1993. Direct simulations of low-Reynolds-number turbulent flow in rotating channel. J. Fluid Mech. 256, 163–197.

Lamballais, E., 1996. Simulations numériques de la turbulence dans un canal plan tournant. Ph.D. Thesis, Institut National Polytechnique de Grenoble.

Lamballais, E., Lesieur, M., Métais, O., 1996a. Influence of a solid-body rotation upon coherent vortices in a channel. C.R. Acad. Sci. 95–101 (Ser. IIb).

Lamballais, E., Lesieur, M., Métais, O., 1996b. Effects of spanwise rotation on the vorticity stretching in transitional and turbulent channel flow. Int. J. Heat Fluid Flow 17 (3), 324–332.

Lamballais, E., Métais, O., Lesieur, M., 1997. Influence of a spanwise rotation upon the coherent-structure dynamics in a turbulent channel flow. In: Chollet, J.-P. et al. (Eds.), Direct and Larde-Eddy Simulation II. Kluwer Academic Publishers, Dordrecht, pp. 225–236.

Launder, B.E., Tselepidakis, D.P., 1994. Application of a new second-moment closure to turbulent channel flow rotating in orthogonal mode. Int. J. Heat Fluid Flow 15 (1), 2–10.

Lesieur, M., 1997. Turbulence in Fluids, 3rd edition. Kluwer Academic Publishers, Dordrecht.

Lin, S., Corcos, G., 1984. The mixing layer: deterministic models of a turbulent flow. Part 3: The effect of plane strain on the dynamics of streamwise vortices. J. Fluid Mech. 141, 139–178.

Métais, O., 1996. Private communication.

Métais, O., Lesieur, M., 1992. Spectral large-eddy simulation of isotropic and stably stratified turbulence. J. Fluid Mech. 239, 157–194.

Ossia, 1997. Private communication.

Piomelli, U., 1993. High Reynolds number calculations using the dynamic subgrid-scale stress model. Phys. Fluids A 5, 1484–1490.

Piomelli, U., Liu, J., 1995. Large-eddy simulation of rotating channel flows using a localized dynamic model. Phys. Fluids A 7 (4), 839–848.

Silvestrini, J.H., 1996. Simulation des grandes échelles des zones de mélange; application à la propulsion solide des lanceurs spatiaux. Ph.D. Thesis, Institut National Polytechnique de Grenoble.

Spencer, B., Jones, B., 1971. Statistical investigation of pressure and velocity fields in the turbulent two-stream mixing layer. In: AAIA 4th Fluid and Plasma Dynamics Conference, Palo Alto, CA, US.

Williamson, J.H., 1980. Low-storage Runge–Kutta schemes. J. Comp. Phys. 35, 48.